energies

MDPI

Article

An Experimental Performance Assessment of a Passively Controlled Wind Turbine Blade Concept: Part B—Material Oriented with Glass-Fiber-Reinforced Polymer

Nikolaos Papadakis * and Constantinos Condaxakis

Power Plant Synthesis Laboratory, Department of Mechanical Engineering, Hellenic Mediterranean University, 71410 Heraklion, Greece; condax@hmu.gr

* Correspondence: npap@hmu.gr; Tel.: +30-2810-379722

Abstract: This paper is the second in a two-part series presenting preliminary results on a passively controlled wind turbine rotor system using a flexible curved blade concept. Building on the initial findings, this segment explores the application of glass-fiber-reinforced polymer (GFRP) composites with strategically oriented layers to enhance blade flexibility and aerodynamic performance and ensure operational safety. Previously, we demonstrated that flexible blades fabricated from isotropic materials with an NACA4415 airfoil profile could self-regulate rotor RPM and power output in response to aerodynamic loads, offering a glimpse of controlled operational behavior, in contrast to straight blades of similar material geometry and aerodynamic characteristics. However, they did not fully meet the design objectives, particularly in achieving nominal power at the intended wind speeds and in safely halting operation at high wind speeds. The current study employs a GFRP blade with a simpler, flat geometry due to manufacturing constraints, diverging from traditional airfoil contours to focus on material behavior under aerodynamic loads. Despite these changes, the blade exhibited all desired operational characteristics: quick startup, stable power output across operational wind speeds, and effective shutdown mechanisms at high speeds. This success illustrates the potential of passively controlled blades designed with appropriately oriented composite layers. Challenges with load application methods—that were identified in the first installment—were addressed by adopting a generator connected to a rheostat, offering improved control over load variations compared to the mechanical brakes used previously. This advancement enabled more consistent data collection, particularly at lower Tip–Speed Ratio (TSR) values, although real-time control for maximum power point tracking was still out of reach. These findings not only confirm the effectiveness of the flexible blade concept but also highlight the need for further refinement in blade design and testing methodology to optimize performance and ease of manufacturing. Future work will continue to refine these designs and explore their scalability and economic viability for broader applications in wind energy technology and in particular to those of small Wind Energy Converter Systems (WECSs).

Keywords: passive control; aero elastic tailoring; adaptive blades; curved blades

check for updates

Citation: Papadakis, N.; Condaxakis, C. An Experimental Performance Assessment of a Passively Controlled Wind Turbine Blade Concept: Part B—Material Oriented with Glass-Fiber-Reinforced Polymer. *Energies* **2024**, *17*, 3286. https://doi.org/10.3390/en17133286

Academic Editors: Cristian Paul Chioncel and Gelu Ovidiu Tirian

Received: 29 April 2024
Revised: 26 June 2024
Accepted: 27 June 2024
Published: 4 July 2024

Copyright: © 2024 by the authors. Licensee MDPI, Basel, Switzerland. This article is an open access article distributed under the terms and conditions of the Creative Commons Attribution (CC BY) license (https://creativecommons.org/licenses/by/4.0/).

1. Introduction

1.1. Findings from Part A: Isotropic Materials

In the first installment of this two-part series, we introduced a novel concept in wind turbine technology: a flexible wind turbine blade designed for passive control, aimed at enhancing aerodynamic performance and operational safety. The flexible blade concept is particularly suited for small Wind Energy Conversion Systems (WECSs) because their presence would reduce the cost of an active electromechanical control system [1].

This innovative approach utilizes inherent blade elasticity to allow for bend–twist deformation around its longitudinal axis under bending loads. This deformation is critical

for the blade's ability to self-regulate in response to varying wind conditions, thereby optimizing its power profile without the need for electrical or hydraulic control systems.

The philosophy of passive control in wind energy systems is based on the turbine's ability to respond to excitation loads and the blade's capacity to function as a feedback mechanism, adapting to operational conditions to meet design criteria. The primary design objectives include maximizing power yield, minimizing operational loads, and optimizing control within the WECS. Implementing a passive pitch control philosophy can drastically reduce blade aerodynamic loads and overall structural stress. Turbines equipped with passive pitch-controlled blades could potentially eliminate the need for complex, moving parts found in actively controlled variable-pitch blades. Instead, these blades adjust their geometry in response to aerodynamic loads, combining the benefits of variable-pitch blades—such as responsiveness, maximization of energy yield, and eventually reduced energy cost—with the simplicity of manufacturing akin to fixed-pitch blades. An additional advantage of passive pitch control blades is their quicker response time, presenting a viable solution for enhancing the feasibility of small WECS.

Our initial findings, presented in the first paper, demonstrated several key advantages of this flexible blade design over conventional straight blades. The study highlighted that the flexible blades could cap their maximum rotational speed and mechanical power output at high wind speeds, exhibiting a controlled and sustainable energy production model. Notably, these blades began generating power at lower wind speeds and maintained a stable power output even as conditions became less favorable, showcasing their efficiency and the effectiveness of the passive control mechanisms integrated into the design.

However, the study also uncovered certain challenges. The passive control mechanisms did not activate at the intended wind speeds, revealing a significant gap between design expectations and actual performance. This misalignment, along with observations of a 'hook-like' feature in the Power Coefficient (C_p) versus Tip–Speed Ratio (TSR) behavior under high wind conditions, suggested areas for further refinement.

As we move into the second part of this series, our focus will shift to addressing these challenges through advanced material usage, design optimization, and enhanced testing procedures. We aim to build on the promising foundation laid by the initial study, refining our designs and methodologies to fully realize the potential of passive control in wind turbine blades. This next phase will explore in depth the opportunities from integration of GFPR-composite-layered orientation to improve blade flexibility and performance.

1.2. Literature Review

The literature on the development of wind turbine blades, particularly those crafted from fiber-reinforced polymers such as GFRP, highlights a significant focus on enhancing blade performance through passive control mechanisms. This review underscores the role of composite layup orientations in achieving desired aerodynamic responses and structural efficiencies, particularly through the implementation of bend–twist coupling.

Liebst [2] in 1986 pioneered studies in this area by examining the effects of wind gusts on curved blades. He noted that such blades could autonomously adjust their geometry, specifically by reducing their pitch angle, thus mitigating aerodynamic loads significantly. This early work set the stage for further exploration into blades that could passively adapt to varying wind conditions. Subsequently, Infield and Feuchtwang in 1995 [3] and in 1999 [4] introduced the concept of "stretch–twist coupled" blades, which were designed to control rotor behavior in runaway scenarios. Their innovative use of a helical layup incorporating both glass and carbon fibers proved effective, as demonstrated by their experimental results aligning closely with predictive models.

Furthering this research, Lobitz and Veers [5,6] conducted studies throughout the late 1990s, focusing on how twist–bend coupling could enhance annual energy production and ensure stability in utility-sized rotors. Their findings revealed that even minor blade twists could result in significant increases in energy output and provided insights into managing

common stability issues like flutter and divergence. Similarly, Eisler and Veers [7] examined adaptive blades on a 26 m diameter variable speed rotor.

The ability of bending twist-coupled blades to attenuate (or exacerbate) the cyclic loading has been investigated by Lobitz and Laino [8], in 1999, and Lobitz, Veers, and Laino [9] in 2000 for a 33 m diameter rotor employing three different control strategies: constant speed stall-controlled, variable speed stall-controlled, and variable speed pitch-controlled. Results for the constant speed stall-controlled case indicate that twist-coupling toward stall produces significant increases in fatigue damage, and for a range of wind speeds in the stall regime apparent stall flutter behavior is observed.

The early 2000s saw continued advancements with researchers like Zuteck [10] exploring the passive control capabilities of bend–twist coupling in larger blades. His work emphasized the necessity of reducing torsional stiffness to enable sufficient blade twisting, suggesting that such designs could also support larger rotor diameters and thus lower energy costs. This line of inquiry was extended by Larwood and Zuteck [11], who compared backward-swept blades to traditional designs, finding improvements in energy capture without additional mechanical strain on the turbine.

Sandia National Laboratories [12] further built on these concepts with their sweep-twist adaptive rotor (STAR) technology, which aimed to enhance rotor efficiency by incorporating passive twisting in blade designs. Their findings demonstrated notable increases in energy capture without exacerbating blade root bending moments, marking a significant step forward in rotor design.

Moreover, the research community has persistently explored optimizing composite ply structures to maximize the mechanical coupling effects. Earlier studies [13,14] and more recent analyses [15] have investigated optimal configurations of bidirectional layups that balance structural integrity with dynamic performance. Tsai and Ong [16] specifically addressed the optimal angular orientation of fibers to maximize bend–twist coupling, pinpointing a 20-degree orientation relative to the span-wise axis as the most effective for certain blade cross-sections.

These collective efforts in the literature underscore a continuous strive towards refining wind turbine blade designs through innovative material use and structural strategies, setting a firm foundation for further advancements in this field. This historical context serves as a critical backdrop for the current study, which aims to push the boundaries of wind turbine blade technology by exploring the integration of GFRP in non-traditional blade configurations, assessing their viability and performance in modern wind energy applications.

1.3. Scope

This second installment of our study series delves deeper into the exploration of novel wind turbine blade designs by examining a curved blade with a rectangular cross-section made from layered Glass-Fiber-Reinforced Polymer (GFRP) in preferential orientation. This design is a departure from the first installment, which focused on a curved blade with a conventional NACA 4415 airfoil cross-section crafted from isotropic materials. The use of a simple, non-airfoil, rectangular shape cut directly from a sheet of composite material signifies a shift towards more practical and cost-effective manufacturing processes within a research laboratory setting.

The decision to utilize a rectangular cross-section arises from the necessity (recognized from the previous installment) to enhance blade flexibility and is driven by the limitations of our current simulation tools, which are not yet capable of accurately predicting the aerodynamic behavior of complex curved shapes with oriented GFRP layers. This simpler shape allows for investigation of the strategic orientation of GFRP layers without the need for creating multiple molds for shaping and curing, significantly reducing both the complexity and the cost of blade production. Such an approach facilitates rapid iterations and modifications, crucial for advancing blade technology through experimental research.

While adopting a non-airfoil shape inevitably leads to certain performance trade-offs, such as reduced aerodynamic efficiency and altered lift-to-drag ratios, this study

primarily focuses on evaluating the mechanical performance of the blade under operational conditions. We aim to assess whether the increased mechanical flexibility, achieved through the preferential orientation of GFRP layers, can be tailored in order to meet specific design goals: achieving a tailored startup at lower wind speeds, maintaining stable power output between nominal and cutoff speeds, and safely stopping the turbine when wind speeds exceed operational thresholds.

The overarching goal of this research is to provide preliminary findings on the effectiveness of using layered GFRP composites in enhancing the flexibility of wind turbine blades. By exploring these non-traditional design and material choices, we hope to offer insights that could benefit small-scale wind turbines or other applications where the ease and cost of manufacturing are more critical than maximizing energy output at an affordable cost. Ultimately, the results from this investigation may open new avenues for future studies into unconventional blade shapes and materials, potentially broadening the scope of design strategies in small wind turbine converter systems and supporting the evolution towards more sustainable and adaptable energy solutions.

2. Methodology

2.1. Overview

In this study, we aim to explore the potential of tailoring the orientation of layered Glass-Fiber-Reinforced Polymer (GFRP) materials to influence the bend–twist deformation of a wind turbine blade, thereby tailoring its aerodynamic performance. This paper presents wind tunnel results for a single curved layered GFRP blade with a rectangular cross-section, selected as the optimal from a series of specimens. The focus of our analysis is on the power versus wind speed tests and the Coefficient of Power (C_p) versus Tip–Speed Ratio (λ). The objectives are threefold: to achieve nominal power output at nominal wind speed, maintain this output between nominal and cutoff speeds, and halt the blade operation when wind speeds exceed safe operational thresholds.

To this end, several blade specimens with varying layer counts and dimensions were fabricated. Of these, we present results from the specimen designated as number 010, identified as the optimal design based on preliminary tests. This specimen measures approximately 155 mm in length, and when mounted on the rotor hub—which has a diameter of approximately 55 mm—the tip's radius extends to 172.5 mm.

The methodology section of this paper will provide a comprehensive overview of the experimental approach undertaken to evaluate the aerodynamic performance of the optimized blade. Although a detailed discussion of the Blade Geometry Algorithm is beyond the scope of this paper, as it will be covered extensively in a subsequent study, we direct the interested reader to the first part of this series which provides an overview. This will set the stage for a deeper understanding of the blade design principles under investigation.

Furthermore, we will detail the test campaign executed for these blades, emphasizing the experimental setups and key findings. This includes a thorough description of the measurement apparatus and the configuration of the wind tunnel used during the tests. By presenting these methodologies, this paper aims to provide clear insights into the experimental procedures and the rationale behind the design choices, supporting the validity of the results obtained from this innovative study.

2.2. Blade Geometry Algorithm

Figure 1 introduces the core concept by comparing straight and curved blades. The curved blade is divided into three sections: the root section, the control section, and the tip section. The root section, which constitutes 25% of the blade length, is engineered for high rigidity to ensure stability. The control section, making up 50% of the blade length, is designed for necessary elasticity to facilitate aerodynamic control. The tip section, comprising the remaining 25% of the blade length, is optimized for enhanced elasticity to respond quickly to wind changes. This segmentation ensures that each part of the blade performs optimally under varying operational conditions.

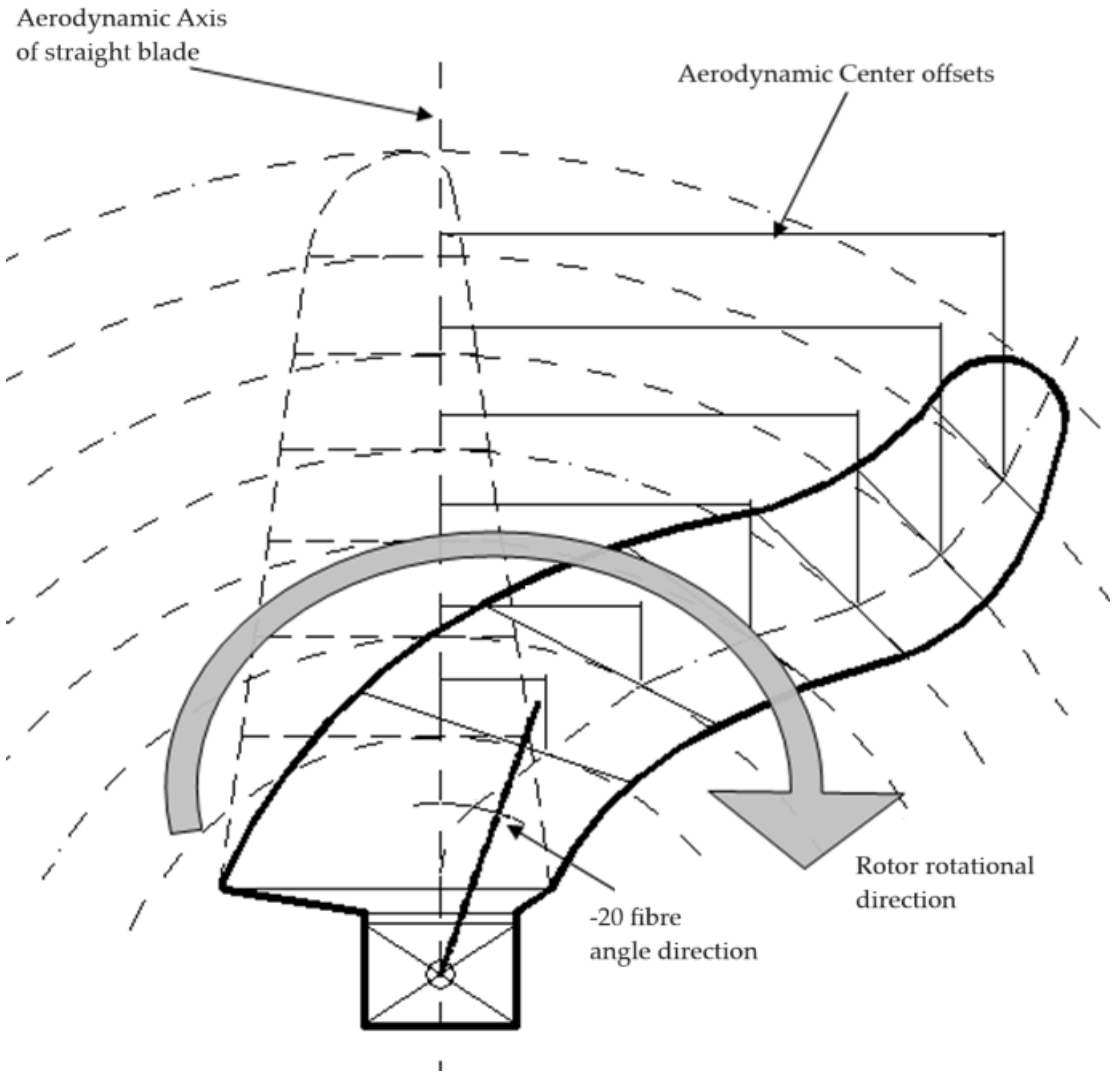


Figure 1. Eccentricity at each section of an early iteration of the curved blade.

The curved blade uses the same aerodynamic cross-sectional profiles as the straight blade, but the profiles for the curved blade are offset by specific angles at different radii. This introduces torsional deformation without altering the chord length or other geometric characteristics, maintaining consistent aerodynamic properties. The offset induces bend–twist coupling under aerodynamic loads, affecting the torsional response of the curved blade.

Part A of this series [17] provided a detailed examination of the aerodynamic behavior of wind turbine blades under various conditions utilizing the NACA4415 airfoil profile. It highlighted how blade geometry interacts with wind conditions to achieve specific aerodynamic responses. For instance, entering aerodynamic stall under high wind speeds helps prevent damage and maintain efficiency. Key design criteria include quick startup to respond to changing wind conditions, achieving nominal power output at nominal wind speeds, maintaining stable power output from nominal to cutoff speeds, and initiating stalling mechanisms at high wind speeds to prevent damage.

Figure 2 provides an overview of the curved blade geometry derivation algorithm and the various steps involved. Initially, a straight/rigid blade is designed using geometry derived from an aerodynamic code. This code incorporates the Larsen, Frandsen, Soeresen, and Courtney [18] theoretical framework for aerodynamic behavior modeling. Additionally, it utilizes enhancements based on Glauert's theory for airfoils and airscrews as described in Désiré Le Gouriérès's "Les Éoliennes" [19] and incorporates aspects of the Hansen

Blade Element Momentum method [20]. Key parameters include nominal power, wind speed, radial chord length distribution, and pitch angle distribution, with adjustments possible to enhance algorithm precision. The curved blade geometry builds on these parameters with the addition of eccentricity, which increases torsional loads and rotations. The process involves modifying profile segments based on initial eccentricity assumptions, calculating bending-torsional deformation using finite element analysis, and optimizing blade geometry in CAD software (Solidworks 2020).

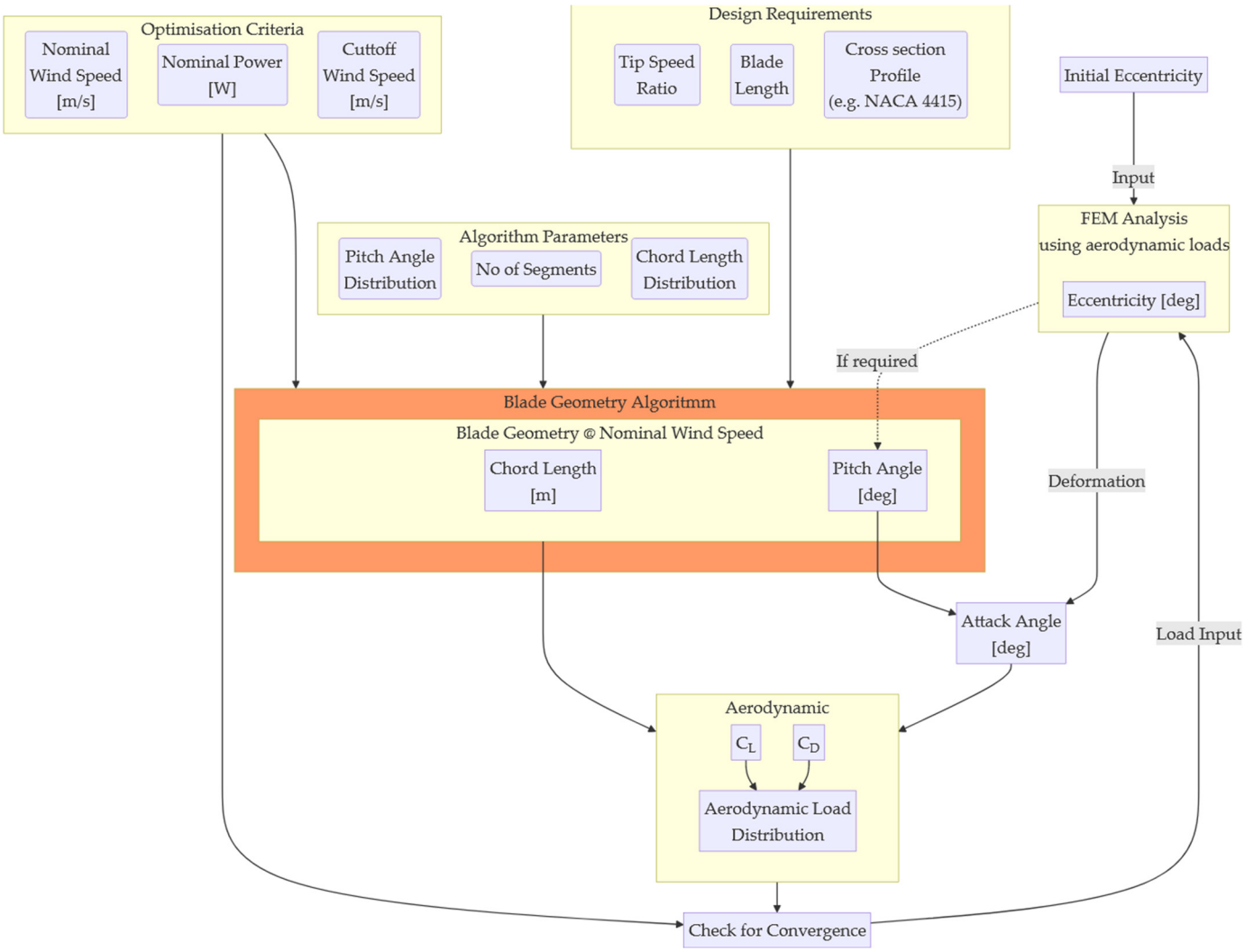


Figure 2. Curved blade design algorithm overview.

Structural analysis in Dassault Solidworks involves fixing the blade edge to the hub, applying aerodynamic loads, and measuring deformation. The blade edge attached to the hub is fixed in all degrees of freedom, while the opposite edge remains entirely free, without any rotational or translational constraints. Load modeling reflects the dynamic pressure of the wind, adopting an inverse triangular thrust distribution. This load distribution assumes zero pressure load at the blade root and maximum pressure load at the tip, representative of typical operational thrust distribution near rated power. The optimization of eccentricity and chord length is based on experience and expertise. Prototypes are manufactured and tested, followed by iterative improvements.

For a more detailed presentation of the wind blade design algorithm, the interested reader should refer to Part A of this series [17].

2.3. GFRP Blade Materials, Fabrication, and Rotor Assembly

In the development of Glass-Fiber-Reinforced Polymer (GFRP) blades, the design extends beyond just the curved planform geometry to also include the orientation of the composite material layers. Given the complexities of constructing a real model with varying fiber orientations across each section of the blade, a uniform fiber orientation was adopted across the span of the micro model blade. However, incorporating different angle orientations throughout the span could potentially provide additional flexibility tailoring.

The fiber orientation is optimized specifically to maximize torsional blade deformation. As illustrated in Figure 3, the graph demonstrates the relationship between the tip torsional deformation angle and the blade material layer fiber orientation angle. The fiber orientation angle is defined as the angle between the elastic axis of the uncurved blade and the fiber axis.

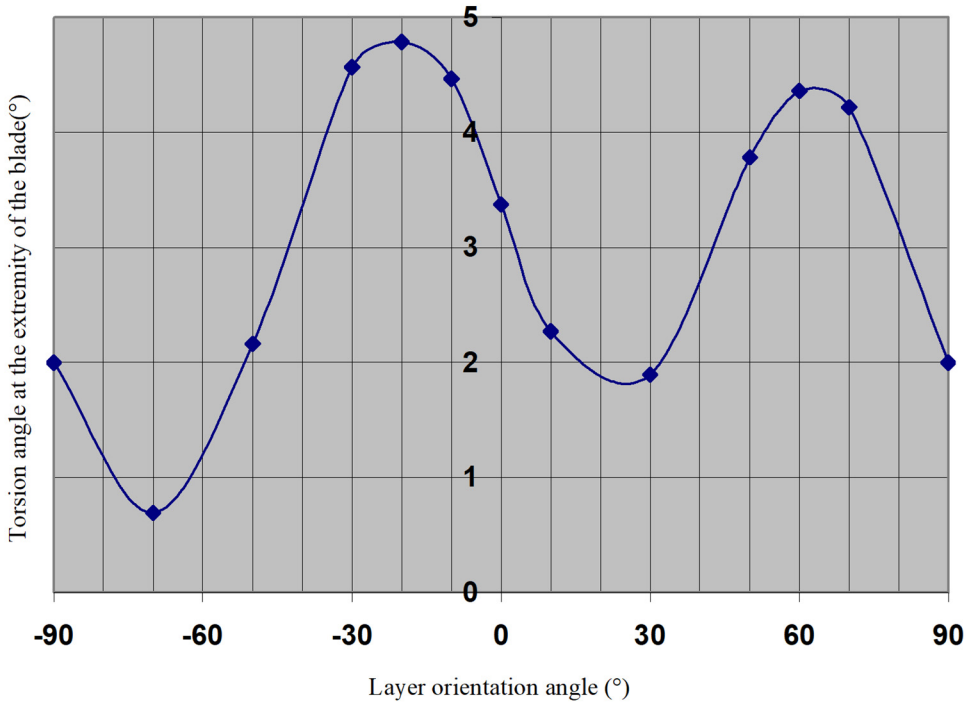


Figure 3. Torsional deformation angle versus the layer fibers orientation angle.

Figure 3 presents the torsional deformation angle versus the layer fiber orientation angle. Simulation results indicate that fiber orientation significantly affects torsional deformation. From −90° to −70°, as well as from −20° to +25° and from 60° to 90°, the torsion angle at the blade's extremity decreases as the layer orientation angle increases. Conversely, from −70° to −20° and from 25° to 60°, the torsion angle increases with an increase in the layer orientation angle. This results in two local minima at angles of −70° and 25° and two local maxima at angles of −20° and approximately 60°. The global maximum occurs at a layer orientation angle of −20°; at this angle, the torsion angle at the blade's extremity reaches 4.79°, correlating with aerodynamic loads at a wind speed of 12 m/s, a finding consistent with other studies [13,14].

For the construction of the GFRP blades in this study, the blades were fabricated from a balanced standard E-glass fabric with a warp/weft ratio of 60/40, weighing 202 gr/m^2, and bonded with an epoxy resin. The construction utilized three layers, though it is important to note that variations in the number of layers can significantly influence both the bending and torsional behavior of the blades. The layers were oriented at 20°, which aligns with the

identified optimal orientation for achieving desired mechanical properties and torsional responses. This orientation results in the following orthotropic mechanical properties:

Young modulus: Ex = 23.5 GPa, Ey = 18.0 GPa, Ez = 18.0 GPa

Poisson's ratio : ν_{xy}= 0.153, ν_{yz}= 0.122, ν_{xz} = 0.153

Shear modulus: Gxy = 4.81 GPa, Gyz = 8.02 GPa, Gxz = 4.81 GPa

To complete the rotor assembly, three blades were fabricated and mounted onto the rotor hub. Due to the manufacturing method—cutting the blades from a sheet of GFRP—it was not feasible to integrate a non-zero pitch angle directly into the blades themselves. Consequently, it was determined that the rotor hub would be designed to incorporate a constant 5-degree pitch angle, thereby ensuring that each blade maintained the necessary angle throughout its length. This design approach effectively compensated for the fabrication constraints, allowing for aerodynamic functionality despite the blades' flat profile.

2.4. Measurement Campaign

2.4.1. Types of Measurements

Two distinct types of measurements were employed during the testing phase, categorized based on the wind velocity conditions: constant velocity (internally denoted as "rr") and increasing velocity ("vv").

Constant Wind Velocity Test: In the constant wind velocity test, the wind blade is exposed to a steady wind until the revolutions per minute (rpm) of the blade stabilize at an equilibrium. Following this stabilization, an external load is gradually applied to the wind blade shaft, either mechanically (or electrically if the rotor is connected to a generator). This test format is commonly used to characterize wind energy blade performance, particularly for calculating the Power Coefficient (C_p) versus Tip–Speed Ratio (TSR or λ). It is important to note that the magnitude of the load significantly influences the Power Coefficient. Specifically, an excessively high load can stall the blade, while an insufficiently light load may prevent the blade from slowing sufficiently to observe the desired effects. During these tests, the braking load is gradually increased to a point where the blade decelerates enough to eventually stop.

Increasing Velocity Test: Contrastingly, the increasing velocity test is designed to characterize the performance of the wind blade across a broader range of wind speeds and may include the application of braking loads. Although not as typical for standard characterization, these tests are crucial in this context as they highlight the benefits of the passively controlled wind energy converter system. This approach allows for an assessment of the blade's adaptability and performance under varying operational conditions.

2.4.2. Measurement Campaign for GFPR Blades (Curved)

Table 1 outlines the key parameters for the measurements of the curved GFRP blade under conditions of increasing velocity. This work reports on four different load settings. Load settings higher than 10 Ohms were excluded from consideration because, under those conditions, the blade failed to initiate rotation. Each test scenario was conducted with a single repetition. During these tests, the wind tunnel velocity was manually adjusted by the operator at a rate of approximately 1 m/s every 10 s, allowing for controlled variations in wind speed.

Table 2 presents the salient parameters for the measurements conducted under constant velocity and constant load conditions using the curved GFRP blade. The tests spanned wind speeds from 4 m/s up to and including 24 m/s, in 2 m/s increments. Two distinct loading methods were employed during these tests.

Table 1. Test parameters for GFRP wind blade (010) VV measurements.

Experiment ID	Resistive Load
58	2
59	4
60	6
62	10

Table 2. Test parameters for GFRP wind blade RR measurements.

Nominal Wind Tunnel Velocity	Ramp Load Experiment ID	Step Load Experiment ID
4	47	66, 80, 106, 132
6	48	67, 81, 108, 134
8	49	68, 82, 110, 136,
10	50	69, 83, 112, 138
12	51	70, 84, 114, 140
14	52	71, 85, 116, 142
16	53	72, 86, 118, 144
18	54	73, 87, 120, 146
20	55	74, 88, 122, 148
22	56	75, 89, 90, 124, 150
24	57	126, 152

The first method involved a ramp load, where the resistive load started at zero and was continuously adjusted upward. This method is referred to as "ramp load", and the corresponding experiment IDs are listed in the second column of the table. The second method, known as "step load", involved incrementally increasing arbitrarily the resistive load in discrete steps and then allowing the rotor hub to stabilize at the new rpm equilibrium. This step-loading method was favored for repeated measurements as it provided more consistent and representative data, capturing the rotor's behavior as it settled into each new load condition.

2.5. Experimental Apparatus

The testing facility for this series of experiments was conducted at the Hellenic Mediterranean University's Wind Energy Lab in a 600 × 600 mm wind tunnel, presented in Figure 4, largely maintaining the setup used in the first part of this series. Despite the similarities in the papers of this two-part series, notable modifications were introduced to address limitations observed in the previously employed braking methods.

The wind tunnel facilitated measurements of various parameters, including wind speed, rotor thrust (T), rotor torque (Q), and rotor speed (N). Table 3 presents manufacturing companies and models of the Measurement apparatus. Wind speed measurements at the tunnel outlet were accurately captured using a Pitot–Prandtl tube coupled with a Delta Ohm HD408T differential pressure transducer, calibrated against an externally calibrated hotwire anemometer to ensure precision. The rotor's axis was connected to a SCAIME DR2112L Rotating Torquemeter, which measured torque and revolutions per minute (rpm). Thrust (or drag) data were collected via an HBM SP4MC6MR load cell interfaced with an ADAM 3016 isolated strain gauge input module. Data acquisition was managed through a National Instruments NI-USB-6353 card, using a custom LabVIEW application developed on the LabVIEW 2014 Development System. This setup allowed data capture at a sampling rate of 1000 Hz for each channel, including measurements for two wind speeds, drag, torque, and rpm, with data segmented into 0.1 s intervals and averaged across each interval.



Figure 4. Wind tunnel at Power Systems Synthesis Laboratory.

Table 3. Measurement Devices.

Measurement	Device	Model Name/No	Company, Country
Wind Speed Static	Differential Pressure Transducer	HD408T	Delta Ohm (Senseca) Padua, Italy
Wind Speed Pitot	Differential Pressure Transducer	HD408T	Delta Ohm (Senseca) Padua, Italy
Torque	Rotating Torquemeter	DR2112L	SCAIME, Haute-Savoie, France
Rotational Velocity	Rotating Torquemeter	DR2112L	SCAIME, Haute-Savoie, France
Drag	Load Cell	SP4MC6MR	HBM (now HBK), Darmstadt, Germany
DAQ	Multifunction Data Acquisition Card	NI-USB-6353	National Instruments, Austin, TX, USA

A significant change in the setup involved the rotor shaft's connection to a small generator, which was linked to a Vishay wirewound rheostat ranging from 0 to 1 k Ohm. This new configuration served as a load on the generator wires, effectively acting as an electromagnetic brake. This modification enabled easy adjustments of the braking load applied to the rotor, facilitating detailed investigations into the generator's performance under varied load conditions.

To ensure that our experimental setup remained robust and reliable and the measurements accurate, each measurement device underwent annual calibration. The calibration procedures involved:

- An externally calibrated hotwire anemometer for wind speeds (already mentioned before).
- Known weights for calibrating the load cell used for measuring drag.
- Standard weights for torque calibration.
- A tachometer to verify the rpm measurements.

3. Results for GFRP Blades

3.1. Geometry for GFRP Blades

Table 4 presents the geometrical characteristics of the GFRP blade (iteration no. 010). As mentioned before, the design starts from a standard straight blade, and an initial eccentricity is applied to the aerodynamical centers of the blade. Then, the aerodynamic loads are applied and a structural analysis is performed in order to determine the torsional angle. Then, adjustments are made on the blade's chord length and eccentricity. Note that the pitch angle that is reported is due to the way it is installed on the rotor (using a wedge with the appropriate), and also note that the radius of the segments is reported from the center of the rotor. The geometry adjustments/optimization procedure currently are human driven using engineering intuition. After several iteration steps (optimization, manufacturing, and testing), the geometry that was tested is presented in Table 4.

The curved blade geometry is presented in Figure 5 (front view and side view) and Figure 6 (side view), and it was expected to develop a twist of 8 degrees at the tip under a

wind speed of 12 m/s. In Figure 6, the eccentricity of the blade and the chord lengths can be seen.

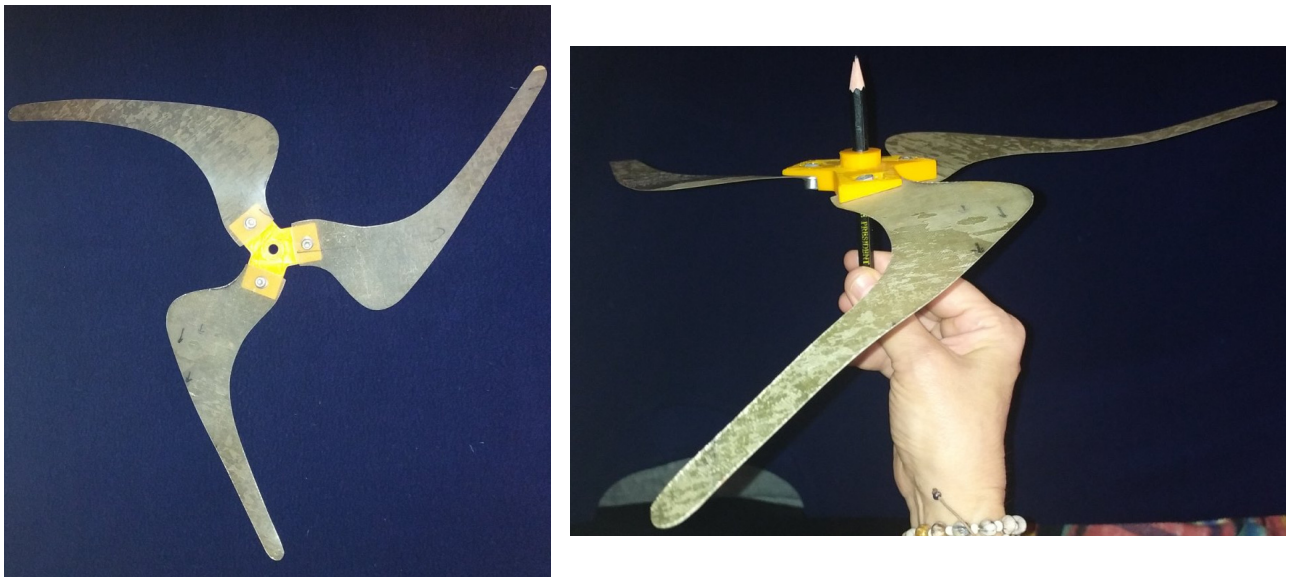


Figure 5. Curved blades assembled on rotor (number 010): front view (**left**) and side view (**right**).

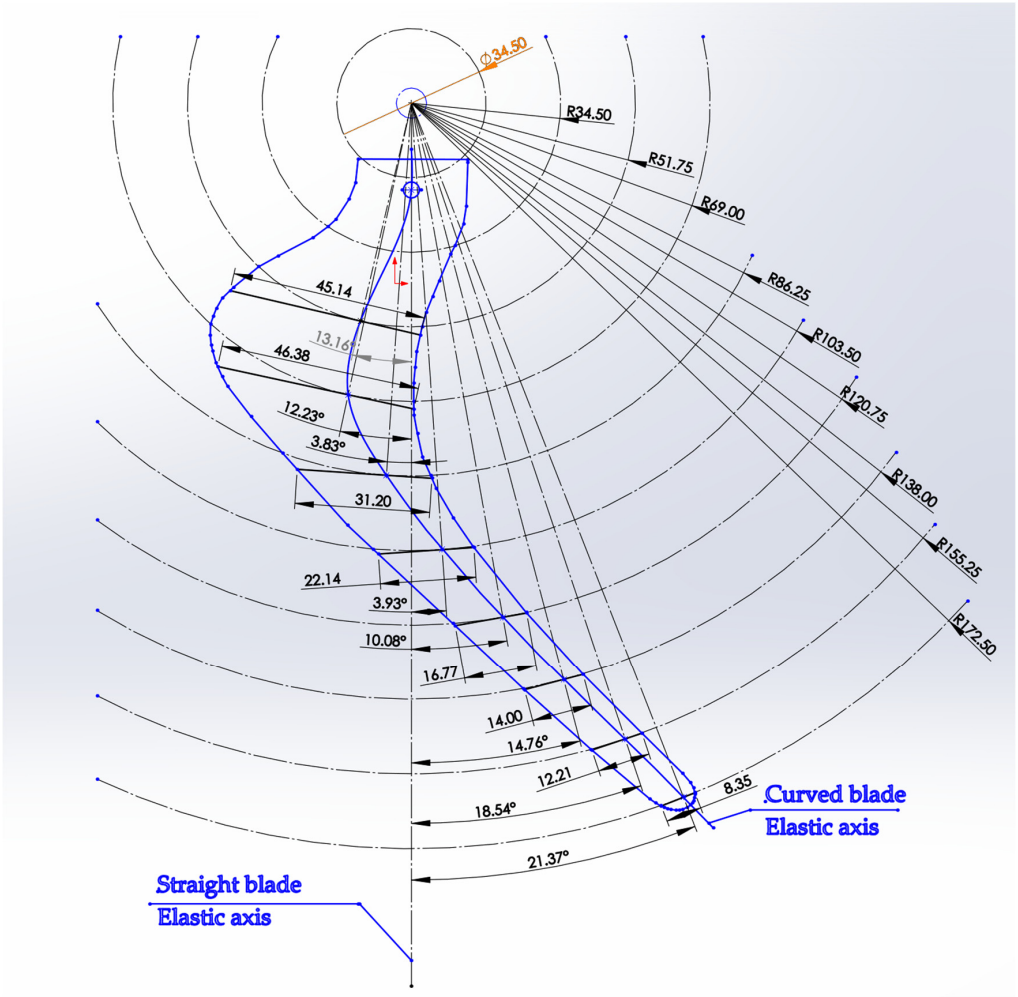


Figure 6. Curved blade geometry (Mk010) with eccentricity details.

Table 4. Geometric characteristics of GFRP blade 010 (center is the rotor hub center).

Seg. No.	Radius [mm]	Chord [mm]	Eccentricity from Elastic Axis [mm]	Eccentricity from Rotor Center [deg]	Pitch Angle [deg]
1	17.25				5
2	34.50				5
3	51.75	45.14	−11.78	−13.2	5
4	69.00	46.38	−14.62	−12.2	5
5	86.25	31.20	−5.61	−3.8	5
6	103.50	22.08	7.09	3.9	5
7	120.75	16.77	21.14	10.1	5
8	138.00	14.00	35.17	14.8	5
9	155.25	12.22	49.37	18.5	5
10	172.50	8.35	62.85	21.4	5

3.2. Increasing Velocity (VV) Measurements

3.2.1. Typical Behavior

Figure 7 presents an automated plot summary from a curved GFRP blade measurement with increasing velocity, used for preliminary data validation. The top graph displays wind tunnel velocity, as measured by the Pitot–Prandtl Tube, which varied from 5 to 24 m/s during this test. The second graph illustrates two variables over time: revolutions per minute (rpm), represented in blue on the primary axis, and mechanical power, depicted in red on the secondary axis. The rpms begin to increase abruptly at 5 m/s, reaching nearly 80% of the maximum value, and continues to rise slowly until the cutoff speed at 22 m/s, where it then drops sharply to zero. Correspondingly, mechanical power, calculated as the product of mechanical torque and angular velocity, increases in tandem with the rpm. The constancy of mechanical power between 5 and 22 m/s suggests that the torque remains approximately stable, as both rpm and power plateau.

The third graph provides a detailed analysis by plotting each power data point against the corresponding wind speeds measured by the Pitot–Prandtl tube, offering insights into the blade's mechanical performance. Notably, this graph shows that beyond 15 m/s, the mechanical power appears to plateau completely, indicating the activation of the passive control features of the flexible curved blade concept.

The final graph displays the Power Coefficient (C_p) against the calculated Tip–Speed Ratio (TSR), derived from wind speed measurements taken by the Pitot–Prandtl tube This graph reveals that the TSR extends beyond 8, and the C_p curve increases non-linearly, following a power-law relationship with TSR. Notably, the higher values of TSR are linked to low wind speeds, arising because the curved GFRP blade starts rotating from rest and rapidly accelerates to 80% of its maximum rpm within a narrow range of wind speeds, leading to observable variability at these high TSR values. It is important to acknowledge that while comparisons of C_p against TSR are typically useful for evaluating different wind blade designs, the results obtained from this study using a blade with a rectangular cross-section cannot be quantitatively compared to those from blades with aerodynamically efficient profiles. Therefore, these plots should be primarily utilized for qualitative analysis.

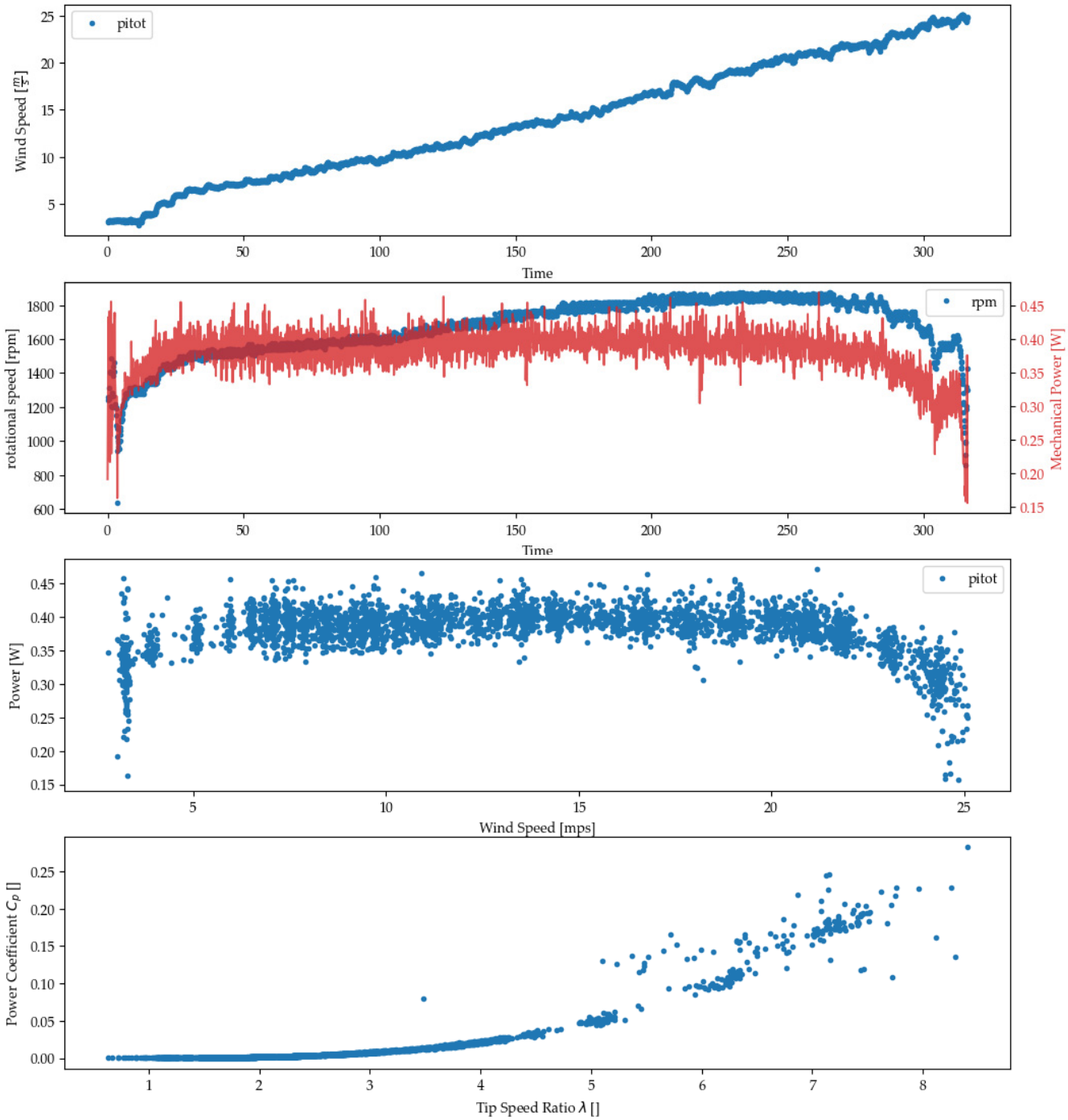


Figure 7. Example of automated plot summary for experiment id 58 (curved blade–GFRP material–vv type–brake resistive load: 4 Ohm).

3.2.2. Power Output Control

Figure 8 displays the mechanical power measurements against wind speed velocity for all increasing velocity tests of the curved GFRP blades, with data points color-coded by brake settings (as resistive loads) and distinct shapes representing different experiment IDs. This figure is pivotal as it illustrates the behavior of the rotor across a range of wind speeds, providing a crucial assessment of how well the curved blade adheres to the established design criteria.

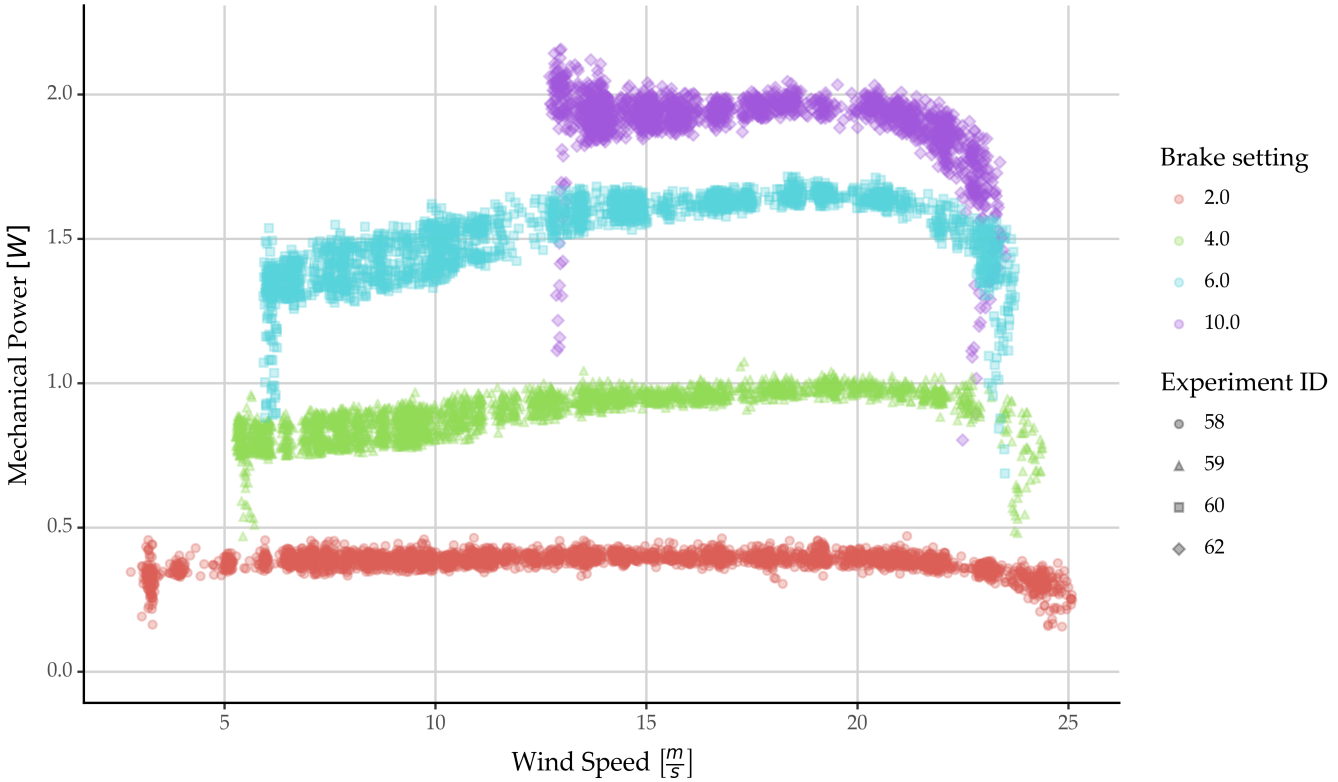


Figure 8. Mechanical power of curved GFRP blade vs. the wind speed (with different load settings).

The graph shows that experiments with higher brake settings result in the commencement of blade rotation at higher wind speeds, which is consistent with observations made with both straight and curved isotropic rotors in the first part of this series. For example, a brake setting of 10 correlates with starting velocities above 13 m/s. Notably, once the rotor starts rotating, a sharp increase in power is typically observed. This behavior indicates that the rotor equipped with the flexible curved blade concept requires overcoming some initial inertia under high load conditions but rapidly achieves nominal power (and rpm) levels once rotation begins, supporting the design criterion for quick startup.

Additionally, the figure demonstrates that with higher brake settings, higher power outputs are observed, suggesting that the rotor can effectively reach and maintain its power output under varying load conditions. Between high speeds, and specifically between the nominal and the cutoff speeds, power output ranges from 70% to 100% of the maximum recorded, indicating that the blade's power output remains stable and predictable, meeting another key design criterion.

A critical observation related to safety is how the blade behaves at cutoff speeds. The graph indicates that beyond certain wind speed thresholds, the rotor's rpm decrease sharply, demonstrating the curved GFRP blade's ability to halt operation under excessive wind conditions to prevent structural damage, thus fulfilling the design criterion for initiating stalling mechanisms at safe operational thresholds. Additionally, it is observed that the cutoff speed increases with decreasing load, likely due to the lower torque values developed by the blade under these conditions.

Overall, Figure 8 is essential for verifying the curved GFRP blade's performance against design expectations, demonstrating its capability to respond effectively to varying wind conditions, manage power output efficiently, and ensure operational safety through appropriate stalling mechanisms.

3.2.3. Rotational Velocity Control

Figure 9 presents the rotational velocity (measured in rpm) of the curved blade against wind speed. This plot demonstrates that the rpm of the curved GFRP blade follow a consistent pattern across all brake settings, with only minor reductions in maximum rpm as the brake load increases, slightly altering the startup and stopping behaviors.

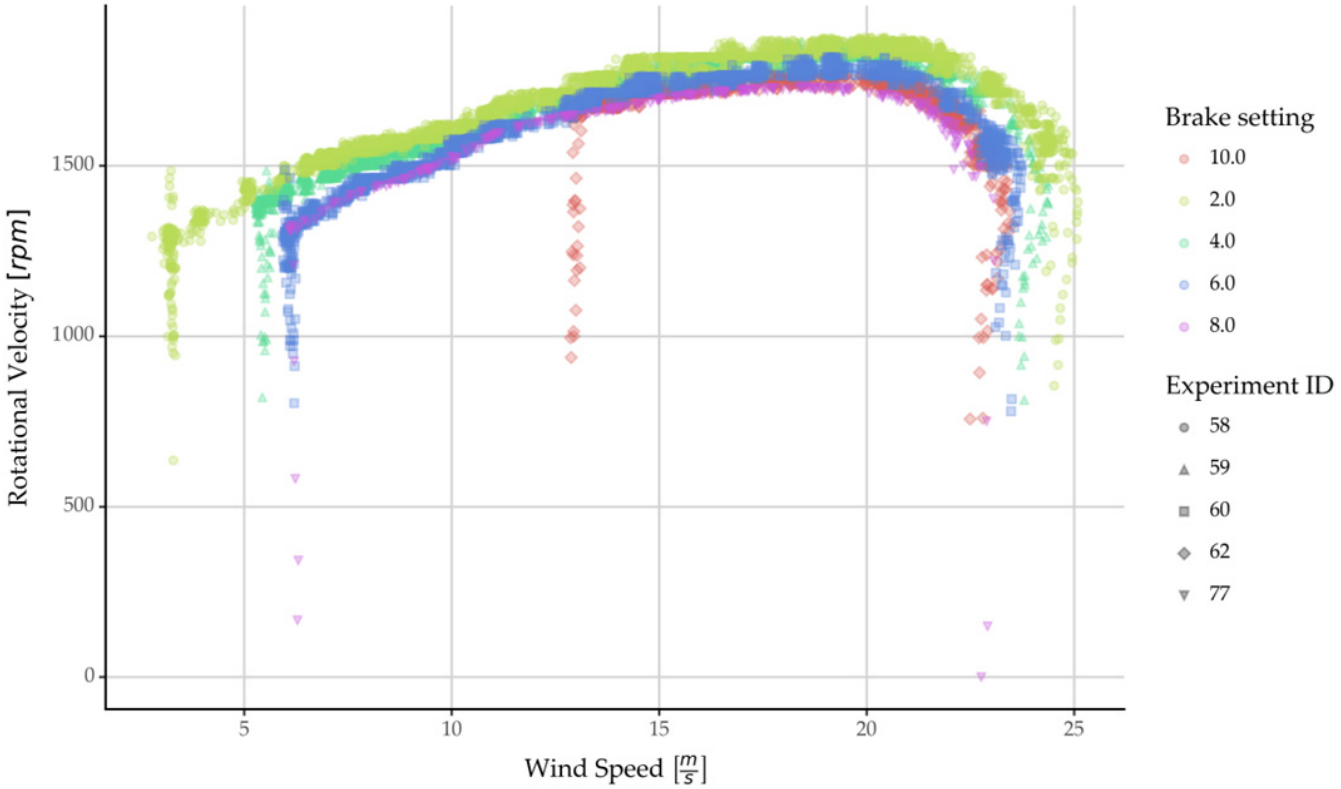


Figure 9. Rotation velocity of blade vs. the wind speed during test (with and without brake).

More specifically, for brake settings ranging from 2 to 8, the rpm increase sharply between wind speeds of 4 and 6 m/s. At the highest brake setting of 10, the rpm do not begin to increase until the wind speed reaches 13 m/s (which also explains why higher brake settings were not utilized).

Additionally, the maximum rpm decrease as the brake load decreases, asymptotically approaching a minimum. This minimum value of maximum rpm is observed at wind speeds of 8 and 10 m/s.

Overall, this data indicate that the rotor equipped with the curved GFRP blade behaves in a controlled and predictable manner regarding rpm, regardless of the brake setting within a certain range of wind speeds. This consistent performance suggests that the desired control features of a WECS can be effectively achieved through the curved GFRP blade design.

Figure 10 depicts the Power Coefficient (C_p) versus Tip–Speed Ratio (TSR) for all increasing velocity tests of the curved blade across different brake settings. Data points are color-coded by brake setting and are differentiated by distinct shapes representing various experiment UIDs. While all brake settings exhibit a trend of increasing C_p with increasing TSR, significant differences are evident among the settings.

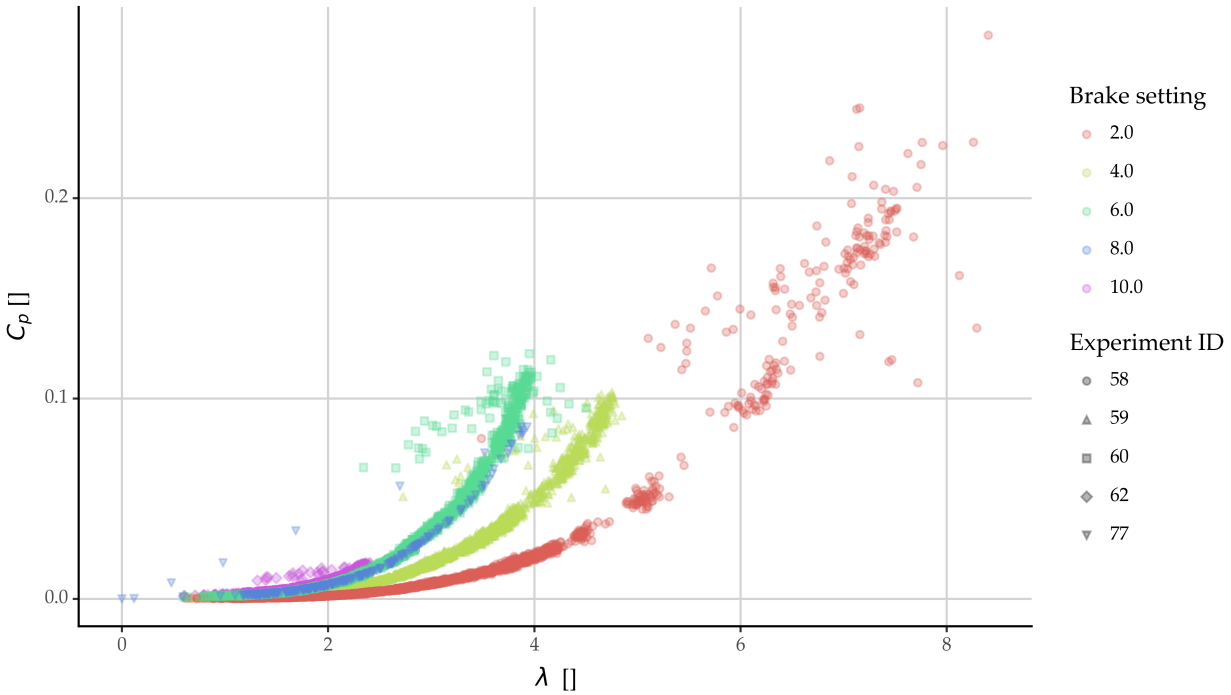


Figure 10. Coefficient of Power with respect to Tip Speed Ratio for curved blade measurements.

Specifically, higher brake settings correspond to lower TSR values and decreased C_p values. This correlation can be attributed to the rapid increase in rpm during startup, which achieves a high proportion of the maximum rpm at very low wind speeds. Due to the rpm increasing quickly within a short timeframe—and thus within a narrow range of wind speeds—the Tip Speed Ratio, defined as $\left(\lambda = \frac{rotational\ velocity}{wind\ speed}\right)$, experiences a fast-changing numerator (which grows to values of 80% of the max rotational velocity) with a relatively stable denominator (which is in the order of 20% of the maximum wind speed). Consequently, TSR values are considerably higher compared to those seen in conventional wind turbines.

Additionally, lower braking settings are associated with higher maximum TSR and C_p values. This is because, under lower loads, the rotor starts to rotate at lower wind speeds, enabling a quicker ramp-up in rotational velocity.

It is important to note that the findings from this plot should primarily be interpreted qualitatively rather than quantitatively. This advisement stems from the fact that such plots are generally more informative under constant velocity conditions, which will be discussed in further detail later in the analysis. This context is crucial for understanding the behavior of the curved blade under variable operational conditions.

In conclusion, the data from this graph further suggest that the curved GFRP blade concept being tested exhibits performance characteristics similar to those found in Wind Energy Conversion Systems (WECSs) with active control systems. Specifically, the rotor equipped with this curved blade design demonstrates a quick startup and maintains relatively constant rpm across a broad range of wind speeds. These findings underscore the potential of the curved blade design to effectively mimic the dynamic response and control typical of actively managed systems, providing a strong foundation for further exploration and development of this technology.

3.3. Constant Velocity (RR) Measurements

3.3.1. Typical Behavior of Constant Velocity (RR) Measurements

Figures 11 and 12 display two automated plot summaries side by side from constant velocity (RR) measurements for experiments with IDs 50 and 69. The key distinction between these plots is that the first graph (exp_id: 50) uses a ramp increase in resistive load,

while the right graph (exp_id: 69) uses a step increase in resistive load. These plots serve as tools for preliminary data validation and are used here to underscore the differences in behavior between ramp load and step load configurations.

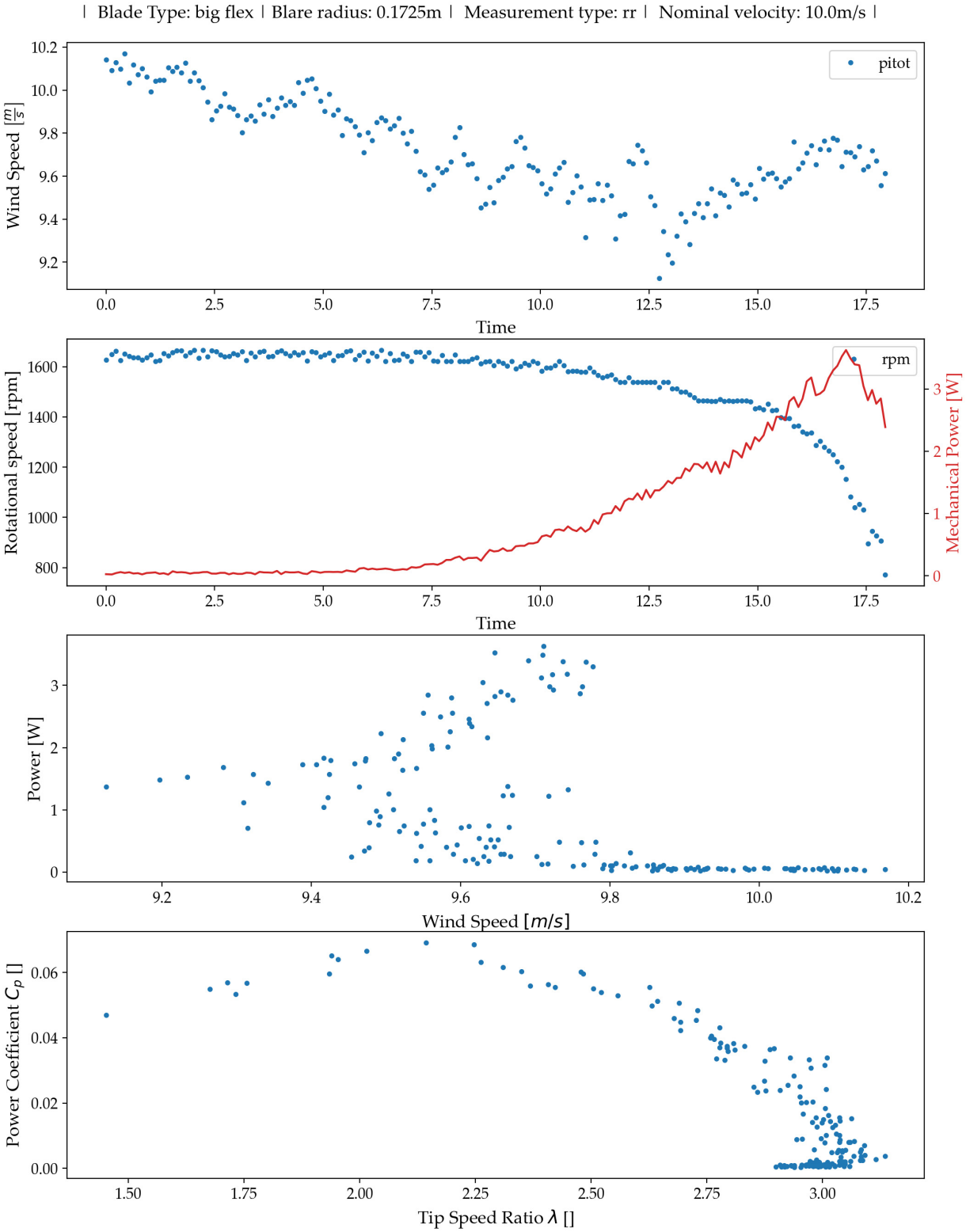


Figure 11. Example of automated plot summary for ramp load: exp_id 50 (flexible blade–GFRP material–rr type–10 m/s–ramp load).

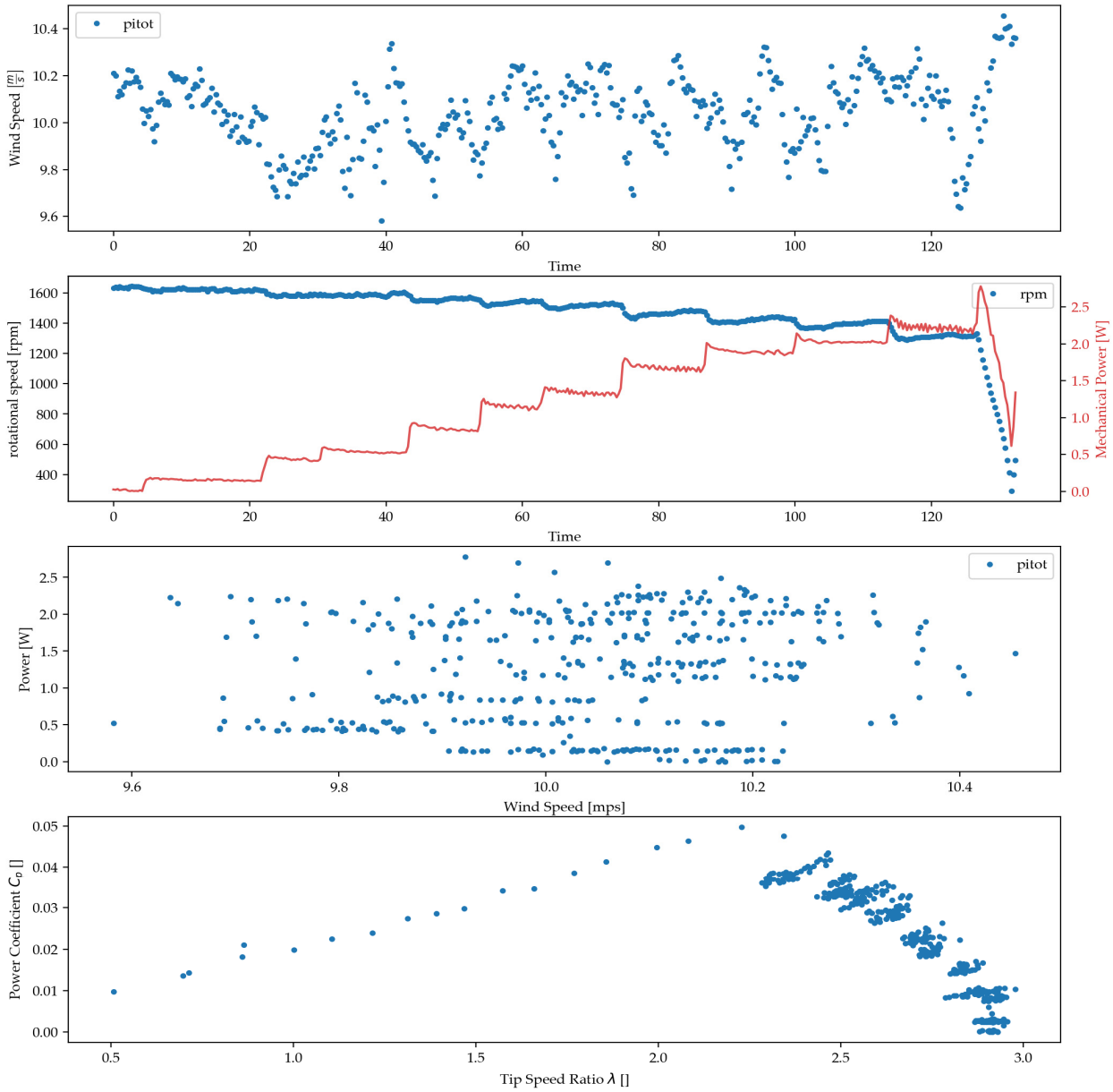


Figure 12. Example of automated plot summary step load for exp_id 69 (curved blade–GFRP material–rr type–10 m/s–step load).

Starting from the top plot, both graphs display wind tunnel velocity from the Pitot–Prandtl tube, which remains around 10 m/s throughout the tests. This velocity shows the typical variability inherent in this type of testing, with no significant differences between the two experiments.

The second graph from the top illustrates the rotational velocity (rpm) on the primary axis and mechanical power on the secondary axis. Here, the impact of the different loading strategies becomes apparent. In the left graph (ramp load), as the brake load gradually increases, the rotational velocity begins to drop, while mechanical power rises until it reaches a critical point where both power and rpm start to decline. In contrast, the right graph (step load) shows that the mechanical power increases in steps, with rpm exhibiting a corresponding stepped decrease.

The third graph, which plots each mechanical power data point against different wind speeds, offers limited informational value due to the narrow range of wind speeds tested.

The final graph at the bottom of the figure depicts the Power Coefficient (C_P) against the calculated Tip–Speed Ratio (TSR), with both scenarios showing a TSR range from 0 to 3. In this graph, the differences between the ramp and step methods are more pronounced. Specifically, in the ramp load scenario, C_P values appear to drop from the maximum towards zero in a less structured manner, whereas in the step load scenario, a pattern resembling inclined lines is observable. These lines illustrate the "settling" of rpm following an abrupt step change in the load. This visualization provides clearer insight into the blade's response dynamics, particularly demonstrating that while the two methods show similar results in the latter half of the TSR range (from the maximum C_p value to the maximum TSR), the step load approach offers more descriptive results in the initial half of the TSR range.

3.3.2. Power Coefficient vs. Tip–Speed Ratio Plots

Figure 13 shows the Power Coefficient (C_p) versus Tip–Speed Ratio (TSR) for all constant velocity tests of the curved blade, with data points color-coded by nominal velocity and grouped by the load type (ramp or step). The black dashed lines are automatically calculated through the Locally Weighted Scatterplot Smoothing (LOWESS) local regression algorithm.

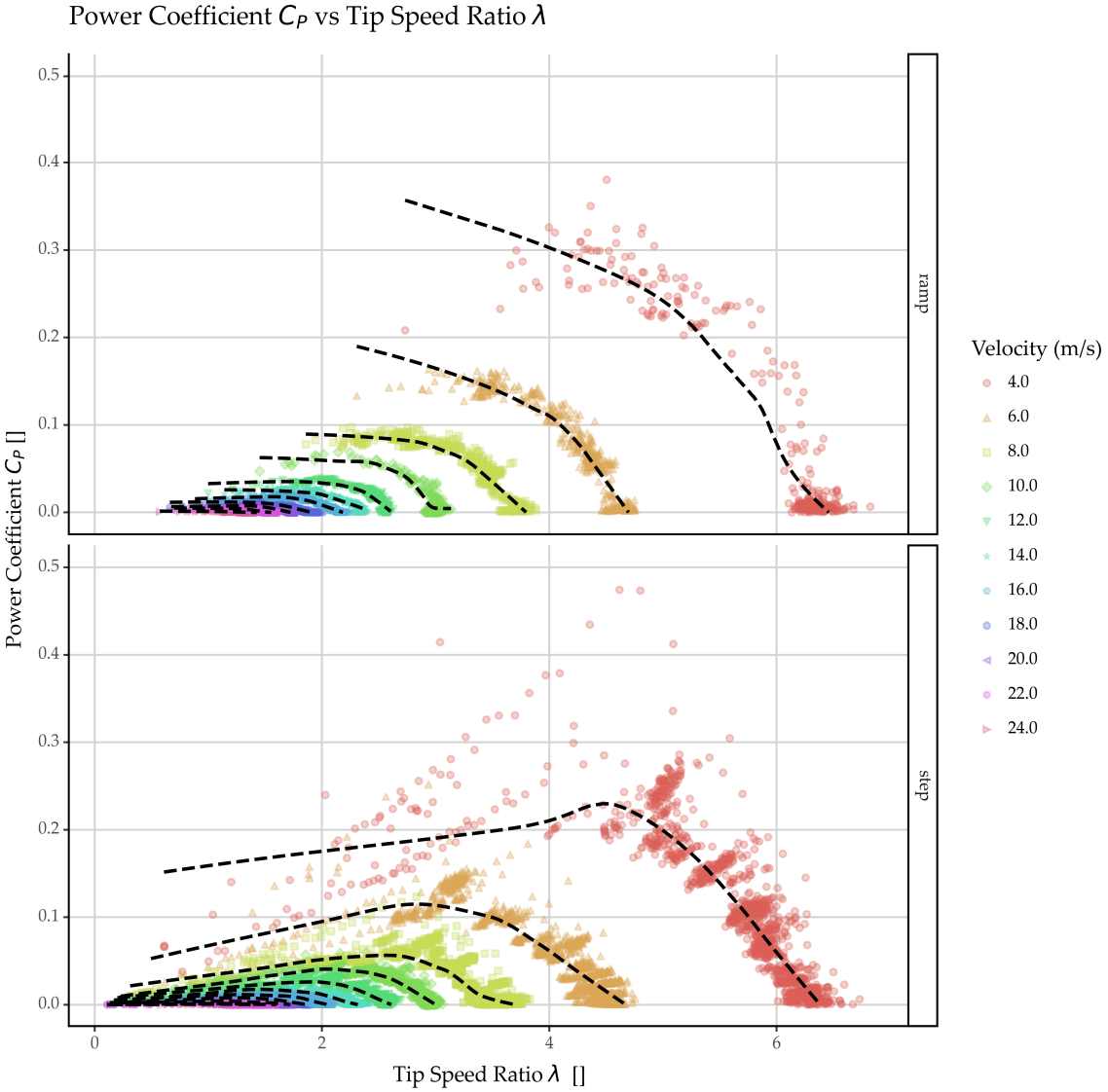


Figure 13. Power Coefficient vs. Tip–Speed Ratio for different velocities of the curved GFRP blade.

A significant observation from this figure is the distinct difference between the ramp and step responses across the TSR range from zero to the maximum value. The step response, which aligns more closely with expected C_p vs. TSR diagrams, was preferred for its repeatability and clearer data patterns. Beyond the maximum TSR value, the responses between the two loading types appear similar. This difference in behavior can be attributed to the stepped response providing more time for the rotor hub to settle into a new rpm equilibrium and stabilize, allowing for more reliable data collection. Conversely, in the ramped load scenario, the rotational velocity decrease is too rapid, resulting in insufficient data capture.

Another prominent feature is that although the maximum C_p values are low compared to conventional wind turbine blade designs, they reach appreciably high levels of about 0.2, particularly at lower wind speeds, which is slightly over one-third of the Betz Limit. The decrease in C_p values with increasing wind speed indicates that less energy is being harvested relative to the available energy in the wind. This pattern, similar to observations in previous sections of this work, underscores the curved GFRP blade concept's ability to initiate rotor hub rotation early and to control and stabilize power output at a nominal level. This performance is akin to that of actively pitch-controlled Wind Energy Conversion Systems (WECSs), suggesting that the curved GFRP blade concept effectively meets the design criteria. This capability demonstrates the potential of the curved blade design to function efficiently in variable wind conditions, emulating some advantages of active control systems while employing passive mechanisms.

3.3.3. Measurement Repeatability

Figure 14 presents displays the Power Coefficient (C_p) versus Tip–Speed Ratio (TSR) for all experiments at a nominal wind speed of 10 m/s, grouped by load type. This graph gives crucial insights for the evaluation of the measurement repeatability. The measurements depicted involve a stepped increase in load, manually adjusted by an operator, which could potentially introduce variability. Despite these challenges, the graph demonstrates that the measurements for the stepped load increases display commendable repeatability across different days, even without a strictly defined protocol. This consistency lends credibility to the reliability of the results.

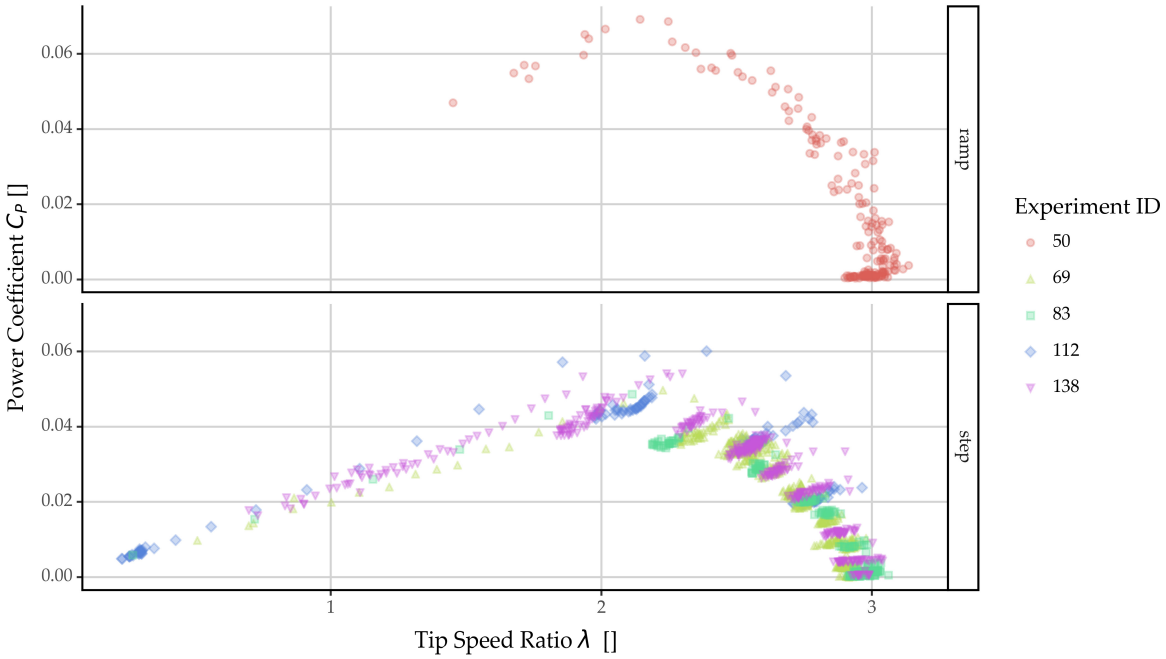


Figure 14. Curved GFPR blade's Power Coefficient vs. Tip–Speed Ratio curve at 10 m/s wind speed for different measurements.

When comparing these results to those obtained under ramped load conditions, the step case typically shows slightly lower C_p values for the same TSR values in the higher TSR range. However, in the lower TSR value range, due to the greater number of measurements taken in the step load case, it provides a more detailed depiction of behavior. This enhanced data collection under step load conditions better illustrates the turbine's performance across a broader range of operational scenarios, underscoring the effectiveness of this measurement approach in capturing the blade performance.

4. Discussion

4.1. General Performance of the GFRP Blade Concept

The performance of the curved, passively controlled GFRP blades developed in this study under a wide range of wind speeds is presented in Figure 15. Three distinct operational regions can be observed: (a) Initial (Buildup) Region, (b) the Second (Plateau) Region, and (c) the Tertiary (Braking) Region.

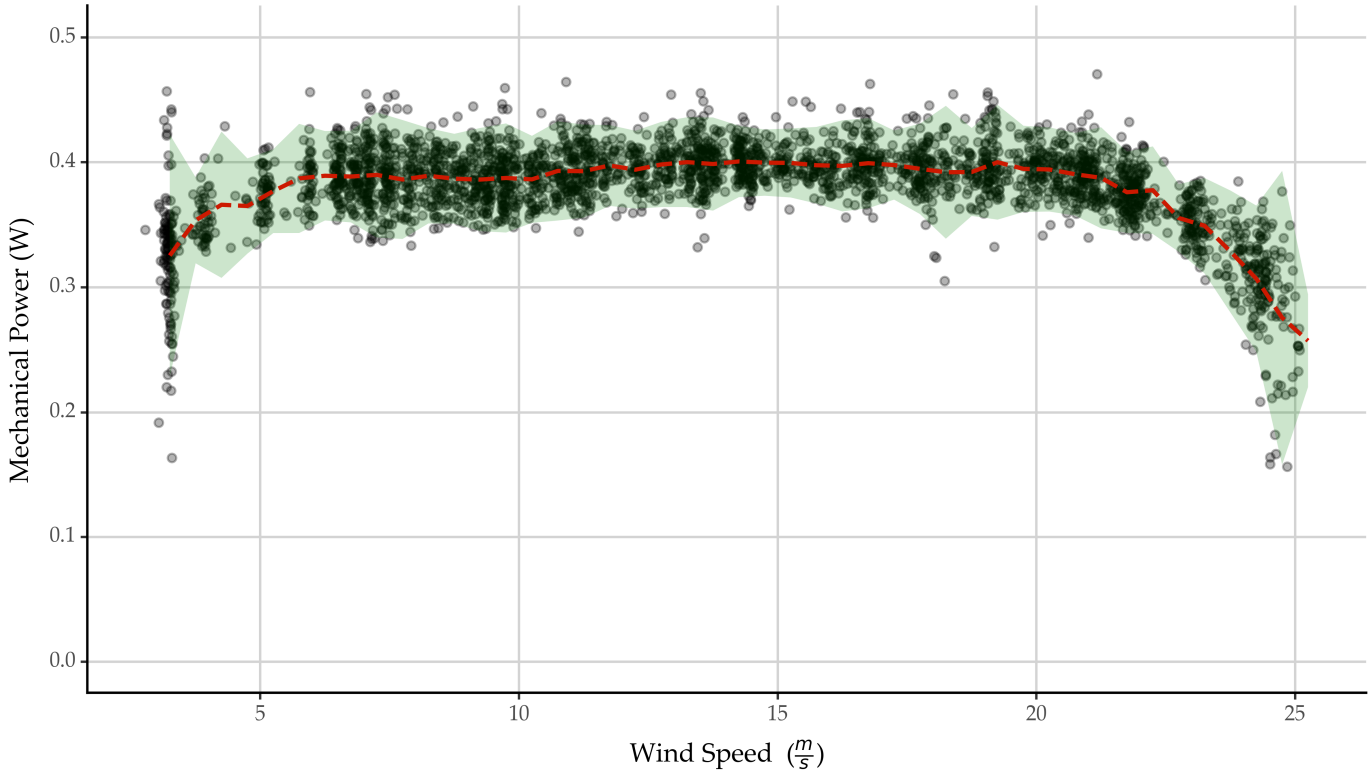


Figure 15. Experiment ID 58 power output vs. wind speed curve at 10 m/s for the passive rotor with diameter 345 mm, 3 layers GFRE, with $\pm 1\sigma$ confidence intervals.

The Initial (Buildup) Region as depicted in Figure 15 spans from 0 to 4 m/s. The curve showing power output versus wind speed begins at zero and rises sharply. The minimal twisting deformations during the early phase are crucial for maximizing torque, which aids in initiating blade rotation. As the curve approaches nominal wind speeds (around 5 m/s in this test), there is a noticeable stabilization in power output. This corresponds to the blade's design feature where the twisting deformation starts to self-regulate. The gradual change in pitch, influenced by the material's elastic properties and blade geometry, modulates the power effectively, preventing any abrupt spikes or drops in energy production as the blade transitions to higher operational speeds. This illustrates how the curved GFRP material and blade design contribute to a controlled and efficient ramp-up in power, aligning with the design criteria for quick startup and efficient energy capture at nominal speeds.

Second (Plateau) Region: This region extends from the nominal wind velocity (5 m/s) to near the cutoff wind velocity (20 m/s). Here, the pitch angle adjusts in response to

increases in wind velocity. As the wind velocity exceeds a desirable level, the pitch angle decreases to deepen the blade's entry into the stall region, thereby reducing power yield. If the power output falls below the nominal level, the pitch angle increases to raise the incidence angle, allowing the blade to gradually exit the stall region. This mechanism is designed to maintain a stable, flat power output curve, which can be observed in the figure.

Tertiary (Braking) Region: Beyond the cutoff wind velocity, this region aims to safely halt the turbine rotation. When the wind velocity exceeds the cutoff threshold, the pitch angle changes significantly, forcing the blade into a deep stall. This action effectively reduces the turbine's rotation until it stops completely. Conversely, if the wind velocity drops below the cutoff threshold, the pitch angle increases, which raises the incidence angle and transitions the blade back into the Second (Plateau) Region to optimize power output.

It should be noted that the actual power output values are dependent on the load setting, as can be seen in Figure 8.

The analysis confirmed that the curved GFRP blade design, despite its simple planar geometry, successfully met all the established design criteria: quick start-up and rapid achievement of nominal power, maintenance of stable power output between nominal and cutoff velocities, and secure shutdown beyond cutoff speeds. This demonstration affirms the curved concept's full capability to meet the functional criteria outlined earlier. This success underscores the viability of designing and manufacturing passively controlled wind turbine blades that could potentially incorporate all the advantages of active pitch and stall control systems found in Wind Energy Converter Systems but with the added benefits of simplicity and cost efficiency inherent in passive systems. While the initial results are promising, there are several considerations for scaling up, which could affect the dynamics and forces involved.

4.2. Resistive Load Setup

To address the limitations identified with the mechanical brake system in the initial study—specifically, its non-linear response characteristics and slow adjustment times which hindered effective power optimization—this study introduced a new approach for applying load to the wind turbine rotor. By integrating a generator connected to a resistive load via a rheostat, we aimed to refine the wind turbine blade testing methodology. The mechanical brake previously used had settings that did not correspond to measurable physical quantities that could be adjusted rapidly, making it challenging to track the optimal power point effectively. The shift to a resistive load was driven by the need for a method that offered more linear and swiftly adjustable load application. Although this innovative approach enhanced the clarity of load-response relationships, the setup still encountered several challenges that affected its capacity to precisely achieve optimal power tracking.

Firstly, the resistive load setup allowed for quick adjustments but did not support real-time digital control, crucial for tracing optimal power values dynamically as wind conditions change. This limitation persisted despite the shift from a mechanical braking system, indicating that further enhancements are necessary to fully capitalize on the potential of this new method.

The load was applied using two distinct methods: a continuous, gradual increase (ramp) and discrete, incremental steps (step). The step-wise method proved particularly effective, as it facilitated more consistent stabilization of the rotor hub's rotational velocity, enhancing data reliability, especially at lower Tip–Speed Ratio (TSR) values. This method also enabled more precise control over experimental conditions, allowing for detailed performance analysis across a broad operational range.

Despite these advancements, the method of manually adjusting the stepped increases by an operator introduced potential variability. However, the results demonstrated commendable repeatability across different testing days, which reinforces the reliability of the findings despite the lack of a strictly defined protocol. Comparatively, the step load conditions typically showed slightly lower C_p values for the same TSR values in the higher

TSR range (see Figure 14); however, it offered a richer depiction of behavior in the lower TSR range due to a greater number of measurements.

Moreover, while the C_p values obtained under ramped load conditions were generally higher, the clarity and control provided by the step approach made it more favorable for consistent data collection. This suggests that while the new loading method has significantly improved the experimental setup, ongoing adjustments and development are required to optimize this system for real-time power optimization and to further enhance the fidelity of data collection for wind turbine performance assessments.

5. Conclusions

This paper is the second installment in a two-part series investigating a novel flexible curved blade concept for wind turbines. In the first part, we fabricated and tested straight and curved blades with NACA4415 airfoil profiles using isotropic polymeric materials. Although the curved isotropic blades demonstrated some desirable control characteristics like fast starting, keeping power output from increasing uncontrollably and ultimately a power plateau beyond critical wind speeds, they fell short of meeting all design criteria. Notably, the nominal power was reached well beyond the nominal velocity, and the blades failed to safely shutdown at or beyond the cutoff velocity. Furthermore, in the first part of the series, the influence of load settings on power measurements and the mechanical brake's inability to track the maximum power point were identified as significant issues.

Building on these findings, this work aimed to explore the potential of adjusting the GFRP orientation to enhance the blade's flexibility, tailor its aerodynamic performance, and meet specific design criteria: quick start-up and rise to nominal power, stable power output between nominal and cutoff velocities, and safe shutdown beyond cutoff speeds. A secondary goal was to explore a different measurement setup that might enable optimal power yield to be obtained at different operating conditions.

To this end, identical GFRP blades with three layers oriented at 20 degrees relative to the blade's longitudinal axis were fabricated from flat sheets of resin-impregnated three-layered GFRP. Each blade measured approximately 155 mm in length and was assembled onto a rotor hub with a final diameter of 355 mm, set at a fixed pitch angle of 5 degrees. This setup was then tested in a wind tunnel.

The methodology employed in this study to arrive at the optimal geometry and layup was labor-intensive and largely intuitive, reflecting the developmental stage of our simulation tools. The process was iterative, with each test cycle refining the blade design and setup based on the previous results. These experiences underline the need for further development of our tools and methods, which will be covered in subsequent publications.

Among various GFRP blades with different geometries and curvatures that were fabricated and tested, results are reported here for blade number 010. The analysis demonstrated that the curved GFRP blade design successfully met all the prescribed design criteria, showcasing that the curved concept is capable of achieving in full the functional criteria that were reported earlier. This success underscores the feasibility of designing and manufacturing passively controlled wind turbine blades that could potentially offer all the benefits of active pitch and stall control Wind Energy Converter Systems but with the simplicity and cost-efficiency of passive systems.

Despite the positive outcomes, this work primarily involved planar geometry as the blade was flat, being cut from a GFRP sheet. The achievement of design criteria with this simple geometry suggests that similar results might be feasible with more aerodynamically efficient cross-sectional profiles, warranting further investigation.

Moreover, a new approach to load application was explored by connecting the rotor shaft to a generator and employing a resistive load via a rheostat. This method provided a clearer and more linear relationship to load application compared to the mechanical brake used previously. Although this approach facilitated quick load adjustments, it did not allow (at least in the first iteration of our setup) for real-time digital control necessary for optimal power point tracking.

Two methods for applying load were explored in this study: a ramp method, where load is increased continuously and gradually, and a step method, where load is applied in discrete increments. Notably, the step-wise method was found to be more effective than the ramped method. It allowed the rotor hub's rotational velocity to stabilize more consistently, which significantly improved data collection, particularly at lower Tip–Speed Ratio (TSR) values. Finally, the Power Coefficient (C_P) values obtained from the ramped approach were generally slightly higher than those from the step approach.

Future Work

Further work in this study will focus on several key areas to enhance the understanding and application of curved wind turbine blade technology. First, there is a need to develop and refine the computational code used for designing and simulating the blades. More detailed presentations of the code will be provided, alongside comparisons between predicted and actual performance metrics. Consideration will also be given to making the code open source, which would facilitate broader collaboration and innovation in the field.

The investigation will continue with an emphasis on the flexible curved blade concept using Glass-Fiber-Reinforced Polymer (GFRP)-oriented materials. Future studies will detail the manufacturing processes, material orientation techniques, and resultant aerodynamic performances of these blades. Comprehensive results from these investigations will be reported to assess the viability and efficiency of the GFRP blades in practical applications.

Another significant aspect of upcoming research will involve a thorough analysis of the thrust/drag forces and the dynamic loading on both the rotor and the blade. There is also an imperative to quantify the flutter and dynamic behavior of the blades under various operational conditions. Although preliminary data are available, detailed studies are required to fully understand these dynamics and implement necessary design adjustments.

Scaling up the design from laboratory or small-scale models to larger, potentially commercial-sized applications is another critical area of focus. This scaling will help in understanding the challenges and adjustments needed for larger turbine implementations.

Additionally, improvements in the experimental setup are planned, particularly the inclusion of a Maximum Power Point Tracking (MPPT) system. Integrating MPPT technology will enhance the capability to precisely find the optimal operational conditions for the turbine systems, thereby maximizing efficiency and output under varying environmental conditions.

Together, these efforts will not only deepen the understanding of flexible wind turbine blades but also push forward the boundaries of renewable energy technology, making it more adaptable, efficient, and applicable on a larger scale.

Author Contributions: Conceptualization, C.C.; methodology, N.P.; software, N.P.; validation, N.P.; investigation, C.C.; resources, C.C.; data curation, N.P.; writing—original draft preparation, N.P.; writing—review and editing, N.P.; visualization, N.P.; supervision, C.C.; project administration, C.C. All authors have read and agreed to the published version of the manuscript.

Funding: This research received no external funding.

Data Availability Statement: Dataset available on request from the authors.

Conflicts of Interest: The authors declare no conflict of interest.

Abbreviations

C_p	Power Coefficient
MPPT	Maximum Power Point Tracking
rpm	Revolutions Per Minute
TSR	Tip–Speed Ratio
WECS	Wind Energy Converter Systems

References

1. Ponta, F.L.; Otero, A.D.; Rajan, A.; Lago, L.I. The Adaptive-Blade Concept in Wind-Power Applications. *Energy Sustain. Dev.* **2014**, *22*, 3–12. [CrossRef]
2. Liebst, B.S. Wind Turbine Gust Load Alleviation Utilizing Curved Blades. *J. Propuls. Power* **1986**, *2*, 371–377. [CrossRef]
3. Infield, D.G.; Feuchtwang, J.B. Design Criteria for Passive Pitch Control of Wind Turbines Using Self-Twisting Blades. *Int. J. Ambient Energy* **1995**, *16*, 139–146. [CrossRef]
4. Infield, D.G.; Feuchtwang, J.B.; Fitches, P. Development and Testing of a Novel Self-Twisting Wind Turbine Rotor. In *1999 European Wind Energy Conference*; Routledge: Abingdon, UK, 1999; ISBN 978-1-315-07433-7.
5. Lobitz, D.W.; Veers, P.S.; Migliore, P.G. Enhanced Performance of HAWTs Using Adaptive Blades. In Proceedings of the Wind 1996 ASME Wind Energy Symposium, Houston, TX, USA, 29 January–2 February 1996.
6. Lobitz, D.; Veers, P. Aeroelastic Behavior of Twist-Coupled HAWT Blades. In *1998 ASME Wind Energy Symposium*; Aerospace Sciences Meetings; American Institute of Aeronautics and Astronautics: Reston, VA, USA, 1998.
7. Eisler, G.R.; Veers, P.S. *Parameter Optimization Applied to Use of Adaptive Blades on a Variable Speed Wind Turbine*; Sandia National Laboratories: Albuquerque, NM, USA, 1998.
8. Lobitz, D.; Laino, D. Load Mitigation with Twist-Coupled HAWT Blades. In *37th Aerospace Sciences Meeting and Exhibit*; Aerospace Sciences Meetings; American Institute of Aeronautics and Astronautics: Reston, VA, USA, 1999.
9. Lobitz, D.; Veers, P.; Laino, D. Performance of Twist-Coupled Blades on Variable Speed Rotors. In Proceedings of the 2000 ASME Wind Energy Symposium, Reston, VA, USA, 10–13 January 2000; American Institute of Aeronautics and Astronautics: Reston, VA, USA.
10. Zuteck, M. *Adaptive Blade Concept Assessment: Curved Platform Induced Twist Investigation*; Sandia National Lab. (SNL-NM): Albuquerque, NM, USA; Sandia National Lab. (SNL-CA): Livermore, CA, USA, 2002.
11. Larwood, S.; Zutek, M. Swept Wind Turbine Blade Aeroelastic Modeling for Loads and Dynamic Behavior. In Proceedings of the WINDPOWER 2006, Pittsburgh, PA, USA, 4–7 June 2006.
12. Ashwill, T.D. *Sweep-Twist Adaptive Rotor Blade: Final Project Report*; Sandia National Laboratories (SNL): Albuquerque, NM, USA; Livermore, CA, USA, 2010.
13. Karaolis, N.M.; Mussgrove, P.J.; Jeronimidis, G. Active and Passive Aeroelastic Power Control Using Asymmetric Fibre Reinforced Laminates for Wind Turbine Blades. In Proceedings of the 10th British Wind Energy Conference, London, UK, 22 March 1988; Milbrow, D.J., Ed.
14. Karaolis, N.M.; Jeronimidis, G.; Mussgrove, P.J. Composite Wind Turbine Blades: Coupling Effects and Rotor Aerodynamic Performance. In Proceedings of the European Wind Energy Conference, EWEC'89, Glasgow, Scotland, 10–13 July 1989.
15. Chen, J.; Shen, X.; Zhu, X.; Du, Z. Study on Composite Bend-Twist Coupled Wind Turbine Blade for Passive Load Mitigation. *Compos. Struct.* **2019**, *213*, 173–189. [CrossRef]
16. Ong, C.-H.; Tsai, S.W. Design, Manufacture and Testing of A Bend-Twist D-Spar. In Proceedings of the 37th Aerospace Sciences Meeting and Exhibit, Reno, NV, USA, 11–14 January 1999.
17. Papadakis, N.; Condaxakis, C. An Experimental Performance Assessment of a Passively Controlled Wind Turbine Blade Concept: Part A—Isotropic Materials. *Energies* **2024**, *17*, 3049. [CrossRef]
18. Larsen, G.C.; Frandsen, S.T.; Sørensen, P.E.; Courtney, M. *Design Basis for Horizontal-Axis Wind Turbines. Theoretical Background*; U.S. Department of Energy: Washington, DC, USA, 1990.
19. Le Gouriérès, D. *Energie Éolienne: Théorie, Conception et Calcul Pratique Des Installations.*; Eyrolles: Paris, France, 1980.
20. Hansen, M. The Classical Blade Element Momentum Method. In *Aerodynamics of Wind Turbines*, 2nd ed.; Routledge: Abingdon, UK, 2007; ISBN 978-1-84977-040-8.

Disclaimer/Publisher's Note: The statements, opinions and data contained in all publications are solely those of the individual author(s) and contributor(s) and not of MDPI and/or the editor(s). MDPI and/or the editor(s) disclaim responsibility for any injury to people or property resulting from any ideas, methods, instructions or products referred to in the content.